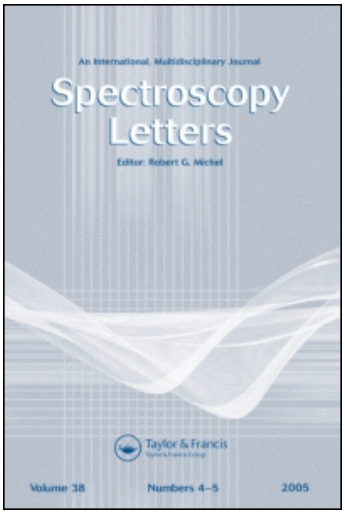

Spectroscopy Letters
Publication details, including instructions for authors and subscription information:
http://www.informaworld.com/smpp/title~content=t713597299

Rotational Dynamics of Excited Probes: Analysis of Rate Constants Based on the Predictions of Hydrodynamic Theory

Bradley R. Arnold[a]; Dustin Levy[a]; Xuefang Lu[a]
[a] Department of Chemistry and Biochemistry, University of Maryland, Baltimore County, Baltimore, Maryland, USA

To cite this Article Arnold, Bradley R. , Levy, Dustin and Lu, Xuefang(2007) 'Rotational Dynamics of Excited Probes: Analysis of Rate Constants Based on the Predictions of Hydrodynamic Theory', Spectroscopy Letters, 40: 1, 149 — 164
To link to this Article: DOI: 10.1080/00387010600853693
URL: http://dx.doi.org/10.1080/00387010600853693

Spectroscopy Letters, 40: 149–164, 2007

ISSN 0038-7010 print/1532-2289 online
DOI: 10.1080/00387010600853693

Rotational Dynamics of Excited Probes: Analysis of Rate Constants Based on the Predictions of Hydrodynamic Theory

Bradley R. Arnold, Dustin Levy, and Xuefang Lu
Department of Chemistry and Biochemistry, University of Maryland, Baltimore County, Baltimore, Maryland, USA

Abstract: The rotational diffusion of benzo(rst)pentaphene (RST) in *n*-hexadecane solvent has been investigated using time-resolved linear dichroism spectroscopy. Theoretical models of rotational diffusion predict biexponential decays of the observed dichroism for this planar polycyclic aromatic probe in solution. Consistent with theory, two time constants of $\tau_1 = 12 \pm 5$ and $\tau_2 = 180 \pm 10$ ps are observed in the loss of dichroism for RST. The ratio of these two time constants is $\tau_2/\tau_1 \approx 15$ and they occur with approximately equal weights within the decay. Hydrodynamic theory, using either slip or stick boundary conditions, would suggest a ratio of only ca. 2–4. Detailed analysis of the preexponential factors for the decay components according to current hydrodynamic theory reveals that there are no physically allowed conditions that would result in a ratio of time constants that exceed ca. 4 while simultaneously allowing the two exponentials to be observed with nearly equal weights within the decay. Based on this finding, it is unlikely that both observed decay components can be due to random diffusional motion.

Keywords: Debye–Stokes–Einstein diffusion theory, fluorescence anisotropy, hydrodynamic theory, polarized spectroscopy, slip boundary, stick boundary

INTRODUCTION

The availability of ultrafast lasers has enabled the development of polarization-specific time-resolved spectroscopic techniques that can monitor the

Received 16 September 2005, Accepted 12 June 2006
Address correspondence to Bradley R. Arnold, Department of Chemistry, University of Maryland, Baltimore County, 1000 Hilltop Circle, Baltimore, 21250, MD, USA. E-mail: barnold@umbc.edu

rotational motions of excited probes directly. These techniques use the anisotropic nature of light absorption to produce partially oriented samples of excited states by a process known as photoselection.[1–7] If such samples are subsequently probed using a second beam of linearly polarized light of wavelength λ, the optical densities observed when the electric vector of the probe beam is parallel ($\Delta OD_{Z(\lambda)}$) and perpendicular ($\Delta OD_{Y(\lambda)}$) to the electric vector of the initial excitation beam may be different. The ratio of these optical densities is known as the linear dichroic ratio, d_λ, and is given by:

$$d_\lambda = \frac{\Delta OD_{Z(\lambda)}}{\Delta OD_{Y(\lambda)}} \tag{1}$$

Other measures used to describe the anisotropic distribution of molecular orientations include the orientation factor, K_λ, which is defined as,

$$K_\lambda = \frac{\Delta OD_{Z(\lambda)}}{\Delta OD_{Z(\lambda)} + 2\Delta OD_{Y(\lambda)}} \tag{2}$$

and the anisotropy, r_λ, as defined by,

$$r_\lambda = \frac{\Delta OD_{Z(\lambda)} - \Delta OD_{Y(\lambda)}}{\Delta OD_{Z(\lambda)} + 2\Delta OD_{Y(\lambda)}} \tag{3}$$

Orientation factors are generally used to describe absorption measurements, whereas anisotropy has been used more frequently when considering emission processes. Conclusions derived from the analysis of experimental data are the same, however, and do not depend on which description is used.

The magnitude of K_λ reflects the extent of alignment of the sample as well as the average projection of the probe transition moment vector (TMV) onto the initial absorption TMV used to excite the sample. Information gleaned from these measurements can be used to study molecular structure,[1–3,7] the distribution of photoproduct structures relative to the orientation of starting materials,[8,9] and the rotational dynamics of molecules in solution.[10–20]

It is well established that the general description of molecular rotational diffusion in solution includes a series of five time-dependent exponential terms.[7,21,22] All five terms are rarely accessible experimentally, and restrictions on their values are possible when molecular symmetry is considered. For example, the TMV projections for π-π^* excited states of planar polycyclic aromatic systems must lie in the molecular plane.[1–3] For molecules of C_{2v}, or higher symmetry, all TMV directions are confined to lie along three mutually orthogonal axes, which will correspond with the symmetry and inertial axes of the molecule.[1–3] As a result of these restrictions on the transition moment vectors for highly symmetric planar probes, the time dependence of polarized π-π^* absorptions will be described completely using a biexponential model function.[7,21,22] In the following report, the principal

symmetry axes will be given the labels L (long), M (medium), and S (short) within the molecular frame of reference (Scheme 1). For high-symmetry probes, the polarized optical densities will be given by

$$\Delta OD_Z(t) = P(t)\left\{\frac{1}{9} + A_1 \exp[-(6D + 2\Delta)t] + A_2 \exp[-(6D - 2\Delta)t]\right\} \quad (4)$$

$$\Delta OD_Y(t) = \left\{\frac{P(t)}{6} - \frac{\Delta OD_Z(t)}{2}\right\} \quad (5)$$

and

$$\Delta OD_{MA}(t) = \frac{\Delta OD_Z(t) + 2\Delta OD_Y(t)}{3} = \frac{P(t)}{9} \quad (6)$$

where

$$D = \frac{1}{3}(D_L + D_M + D_S) \quad (7)$$

$$\Delta = \sqrt{D_L^2 + D_M^2 + D_S^2 - D_L D_M - D_L D_S - D_M D_S} \quad (8)$$

In these equations, $\Delta OD_Z(t)$, $\Delta OD_Y(t)$, and $\Delta OD_{MA}(t)$ are the optical densities observed with the probe beam linearly polarized along the laboratory Z-axis, the Y-axis, and at the magic angle (54.7°) with respect to the Z-axis, respectively, assuming the excitation beam was polarized along the laboratory Z-axis. D_i represents the diffusion coefficient for rotation about the indicated molecular axis where i = L, M, or S. D is the average diffusion coefficient, and Δ is a measure of the degree of rotational anisotropy. The function $P(t)$ in Eqs. 1–3 describes the time dependence of the excited state population. Plots of d_λ, K_λ, or r_λ versus time are independent of $P(t)$ but may require an accurate description of the instrument response function, which can be determined using $P(t)$, if deconvolution of the instrument response is necessary. As can be observed in Eq. (6), the time course of the magic angle trace is independent

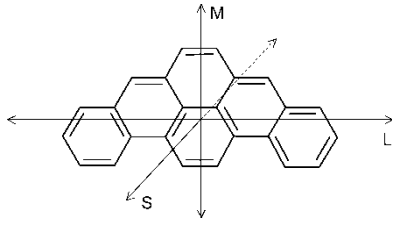

Scheme 1. Benzo (rst) pentaphene (RST).

of the TMV projections and the diffusion coefficients and allows $P(t)$ and the instrument response to be measured in the absence of dichroic effects. In the following report, the magic angle trace will be used to determine the correct form of $P(t)$ and the instrument response functions, which will be used in the subsequent calculation of the individual $\Delta OD_Z(t)$ and $\Delta OD_Y(t)$ traces.

Single exponential model functions [Eq. (9)] are used frequently to describe the experimentally observed dichroism (anisotropy) decays,[16,19,20]

$$\Delta OD_Z(t) = P(t)\left\{\frac{1}{9} + (A_1 \exp[-(6D_{iso})t]\right\} \tag{9}$$

Here D_{iso} is the diffusion coefficient assuming isotropic rotation of the probe with $\Delta = 0$, and Eqs. (5) and (6) are still valid. In an earlier report, we used simulated decay traces assuming stick boundary conditions to predict the relative values of the diffusion coefficients for a general ellipsoid and showed that the simulated dichroism decay traces could be described using single exponential model functions with exceptionally small error.[23] Thus, the appearance of biexponential decays, while predicted by theory, should be unusual in practice because of the inherent noise included in experimental data.

This report evaluates the rotational diffusion of the first excited singlet state of benzo(rst)pentaphene (RST) in *n*-hexadecane using time-resolved linear dichroism spectroscopy. The experimentally determined dichroic decays are evaluated using both the single exponential and biexponential model functions. The results show clearly that a single exponential decay is not sufficient to accurately fit the observed decays and that a biexponential function is the minimum required to accurately fit the data. The time constants obtained from the biexponential fits were evaluated in terms of the hydrodynamic model at different boundary conditions to assess their relationship to the random rotational diffusion of RST.

MATERIALS AND METHODS

Methods

The picosecond pump-probe apparatus used in these experiments has been described in detail elsewhere.[24] A Continuum PY61C Nd:YAG laser (Santa Clara, CA) was used to produce 1064-nm pulses that were subsequently tripled to produce 355-nm pulses for sample excitation. Focusing the 355-nm light into a 25-cm solution cell of water and isolating the resulting stimulated Raman emission allowed excitation pulses at 404 nm to be obtained. White light continuum pulses were generated by focusing 12 mJ of residual 1064-nm light into a 10-cm cell containing a 1:1 mixture of H_2O/D_2O. The typical instrument response was between 40 and 60 ps assuming Gaussian profiles.

An IBM-compatible personal computer allowed automated control of the experiment in addition to data storage and manipulation.

RST and *n*-hexadecane were obtained from Aldrich Chemical Co. (Milwaukee, WI) and were used as received. Solutions of RST were placed in a quartz cuvette with *n*-hexadecane as solvent. Ground state absorption spectra were recorded at 22 ± 1°C using a Beckman DU 640 UV-Vis spectrometer (Fullerton, CA). For time-resolved measurements, the optical densities of the samples at the excitation wavelength were adjusted to a value of 0.2. Decay traces were collected at 22 ± 1°C and were constructed by averaging 200 laser pulse pairs at each delay setting. Samples were stirred using a magnetic stirrer, and no changes to the optical spectra of the samples were observed during the course of the experiment. The resultant time-resolved curves were fit using a custom computer routine to find the nonlinear least squares minimum of the error between a model decay function and the observed data trace.

RESULTS

The ground state absorption spectrum of RST in *n*-hexadecane solvent is shown in Fig. 1. The absorption spectrum of the first excited singlet state is also included in the figure. The excited state spectrum was obtained when the continuum pulse was delayed 5 ps relative to the excitation pulse with the relative polarizations of the two beams at the magic angle. The transient spectrum recorded does not change for delays longer than a few nanoseconds and therefore does not include artifacts due to stimulated emission, triplet formation, or secondary reaction products of the excited state. The ground state and first excited state spectra both exhibit a complex series of vibronic progressions with multiple overlapping electronic transitions.[25]

Magic angle and polarized decay trace sets were obtained using 355-nm excitation with 554- or 640-nm probe wavelengths. These traces are shown in

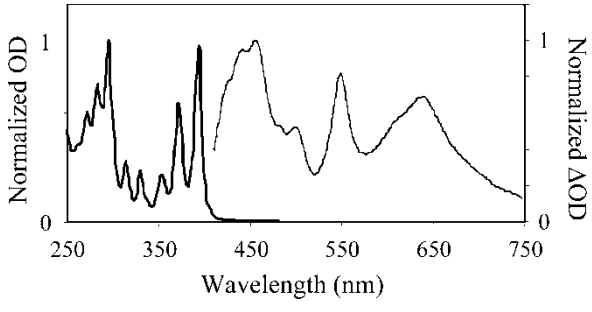

Figure 1. Normalized absorption spectra of the RST ground state (thick line) and the RST excited singlet state in *n*-hexadecane recorded 5 ps after excitation at 355 nm (thin line).

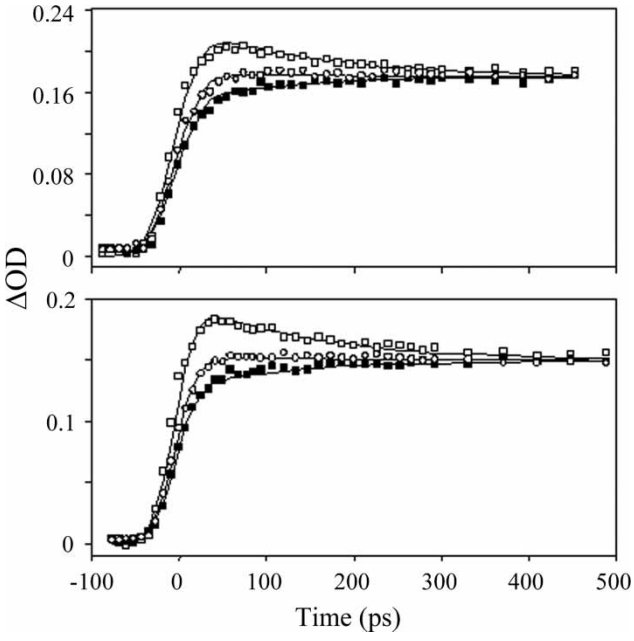

Figure 2. Picosecond pump-probe absorption decays of RST in *n*-hexadecane obtained using 355-nm excitation polarized linearly along the laboratory Z-axis with a 554-nm probe beam (top panel) and a 640-nm probe beam (bottom panel) polarized along the Z-axis (open boxes), Y-axis (closed boxes), and at the magic angle (open circles). The fitted curves represent the best fits of the magic angle trace [Eq. (10)] and the dichroic traces using Eqs. (4) and (5).

Fig. 2. Using otherwise identical conditions, 404-nm light was used for sample excitation, and similar sets of traces at probe wavelengths of 554 and 640 nm were also collected. These traces are shown in Fig. 3.

DISCUSSION

Evaluating *P(t)*

The magic angle decay traces for the RST excited state produced with either 355- or 404-nm excitation and observed at either 554 or 640 nm are shown in Figs. 2 and 3 (open circles). The excitation beam used to produce these traces was linearly polarized along the laboratory Z-axis, and the probe beam was linearly polarized at 54.7° with respect to the laboratory Z-axis. As described above, the magic angle traces do not contain dichroic information but are instead exclusively due to the formation and decay of the RST excited state convoluted with the instrument response function of the laser

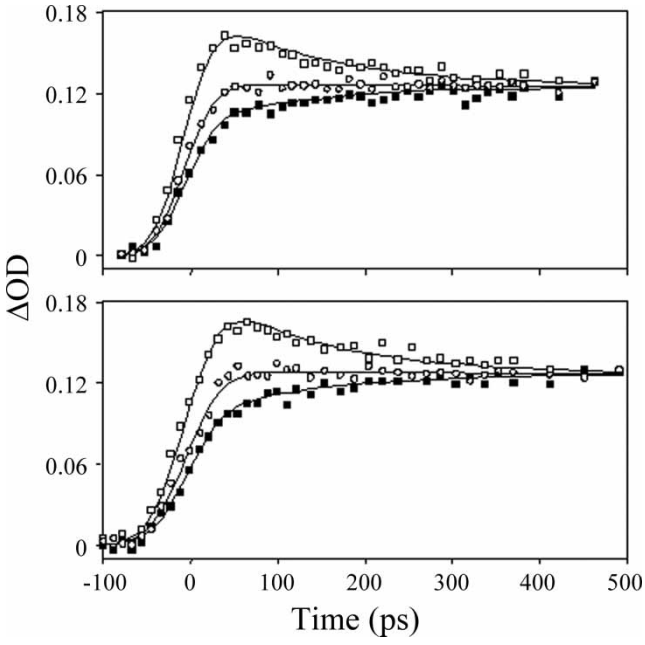

Figure 3. Picosecond pump-probe absorption decays of RST in *n*-hexadecane obtained using 404-nm excitation polarized linearly along the laboratory Z-axis with a 554-nm probe beam (top panel) and a 640-nm probe beam (bottom panel) polarized along the Z-axis (open boxes), Y-axis (closed boxes), and at the magic angle (open circles). The fitted curves represent the best fits of the magic angle trace [Eq. (10)] and the dichroic traces using Eqs. (4) and (5).

photolysis apparatus. Thus, the magic angle traces can be used independently to determine the correct form of $P(t)$.

The magic angle traces were analyzed assuming a single exponential excited state decay according to:

$$P(t) = 9\Delta OD_{MA}(t) = 9A_{MA}\exp[-k_{MA}t] \tag{10}$$

Nonlinear least squares analysis of all four magic angle traces included in Figs. 2 and 3 yielded an average value of $k_{\mathrm{MA}} = 3.43 \pm 1.33 \times 10^7\ \mathrm{s}^{-1}$ with the individual preexponential factors, A_{MA}, given in Table 1. In each case, the instrument response functions were between 40 and 60 ps assuming a Gaussian intensity profile. The best fit of each magic angle trace is included in the figures as a solid line. The 500 ps observation window used in these experiments does not allow the ca. 20–40 ns decay of the excited state to be measured accurately, but the decay constant obtained is consistent with a long-lived excited state as expected for RST.[26] More germane to the current discussion, the parameters obtained from fitting the magic angle data will be used as fixed values to describe the form of $P(t)$

Table 1. Fitting parameters for magic angle and dichroic traces of benzo[rst]pentaphene in *n*-hexadecane

λ_{EX} (nm)	λ_{PR} (nm)	A_{MA} (OD)	k_{MA} (10^7 s^{-1})	A_1[a] (OD)	τ_1[b] (ps)	A_2[c] (OD)	τ_2[b] (ps)	K_i[d]
355	554	0.177	3.43	0.0359	12	0.0493	180	0.493
355	640	0.153		0.0365		0.0482		0.520
404	554	0.127		0.0425		0.0530		0.584
404	640	0.128		0.0507		0.0390		0.567

[a] $\pm 10\%$.

[b] Time constants obtained by fitting all four sets of dichroic traces simultaneously, ± 5 ps.

[c] $\pm 5\%$.

[d] Initial orientation factor, ± 0.03.

and the instrument response function within the analysis of the dichroic decays.

Analysis of Time-Resolved Linear Dichroism Decays

The single exponential dichroism decay model, given by Eqs. (9) and (5), was used to describe the individual dichroic decay traces for RST in *n*-hexadecane. Figure 4 includes the experimental data for excitation at 355 nm and probe of 640 nm displayed as the observed orientation factor as a function of time. To obtain these plots, the polarized traces in Fig. 2 were fit according to the single exponential dichroism decay [Eqs. (9) and (5)] and then the orientation factors were calculated as a function of time according to Eq. (2). The experimental (filled circles) and the predicted (solid line) orientation factor traces are included in Fig. 4 as is the residuals plot obtained as the difference between the experimental data and the predicted orientation factor. The residuals plot shows the unmistakable sinusoidal hallmark of a single exponential fit to a multi-exponential decay. The first few data points are severely underestimated while the next ca. 20 points are generally overestimated and the remaining points, on average, underestimated. Similar residuals plots were obtained after analysis of the remaining data sets. On the basis of the nonrandom distribution of residuals, it was concluded that the RST dichroism decay traces could not be described using a single exponential model function.

When the time-resolved linear dichroism traces were analyzed according to the biexponential model function given in Eqs. (4) and (5), excellent fits to the data were achieved. Each of the four sets of dichroic traces could be fit simultaneously using the same two time constants while the weights of the exponentials were allowed to vary within each data set. Figure 5 includes

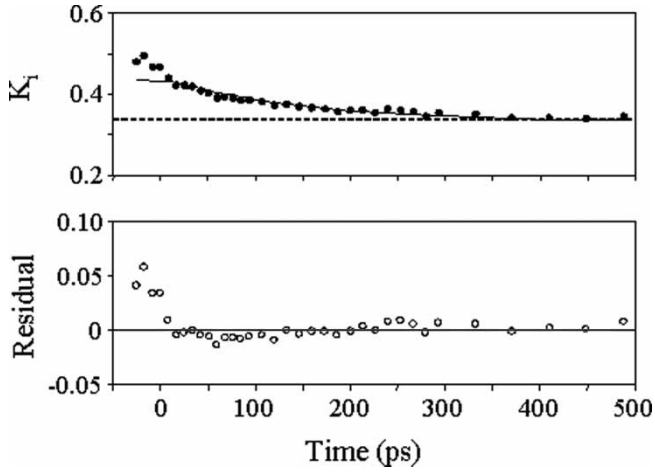

Figure 4. Top panel: Orientation factor decay of RST in *n*-hexadecane observed at 640 nm following excitation with 355-nm light. The fitted curve indicates the best fit according to a single exponential decay model (please see text) displayed as orientation factor, K_i. The dashed line represents the isotropic K_i value of $1/3$. Bottom panel: Residuals plot for the single exponential decay model.

the experimental (filled circles) and predicted (solid line) orientation factor decay and the residuals plots according to the biexponential model for excitation at 355 nm with a probe wavelength of 640 nm. These plots were constructed in the same way as the plots shown in Fig. 4, except that a biexponential dichroism decay was assumed. No systematic errors could be detected in the residual plots shown in Fig. 5, which shows the data points are randomly scattered about the predicted orientation factor. Excellent fits of the remaining three data sets were also achieved, and the decay constants and preexponential factors determined are collected in Table 1.

Although it appears to be a necessary condition to require biexponential decays for dichroic traces of RST, the appearance of a biexponential decay is not sufficient to prove that both decay components are related to the random rotational motions of the probe. For RST in *n*-hexadecane, two time constants are observed as expected by hydrodynamic theory, but it is not yet clear that both time constants describe the random rotational diffusion of the RST excited state. The ratio of the observed time constants falls between the values $\tau_2/\tau_1 \approx 12$ to 20. Similar ratios of time constants have been reported for disk-like perylene[15,17,18] and rod-like tetracene[18] in *n*-hexadecane, as well as coumarin 153 in several solvents.[20] Can such large ratios of time constants be consistent with anisotropic rotational diffusion? To answer this question, the time constants observed experimentally will be compared with those predicted by hydrodynamic theory.

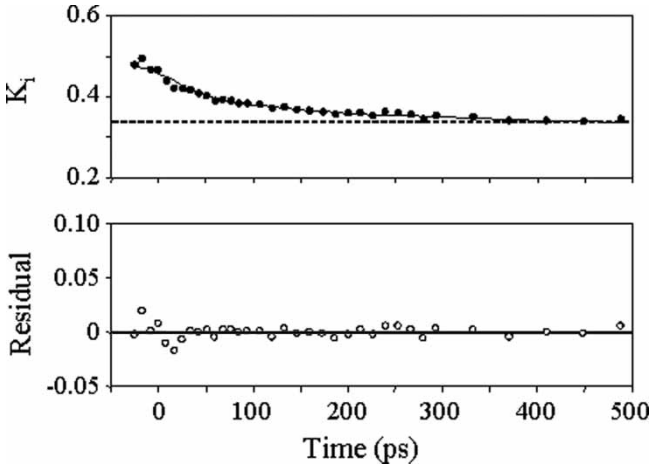

Figure 5. Top panel: Orientation factor decay of RST in *n*-hexadecane observed at 640 nm following excitation with 355-nm light. The fitted curve indicates the best fit according to the biexponential decay model displayed as orientation factor, K_i (please see text). The dashed line represents the isotropic K_i value of 1/3. Bottom panel: Residuals plot for the biexponential fit.

Debye–Stokes–Einstein Theory

Debye–Stokes–Einstein (DSE) theory for diffusional motion[7] attempts to relate solvent properties, specifically viscosity, to the rotational time constants of a probe molecule in solution according to Eq. (8).

$$\tau_{or} = \frac{\eta V}{k_B T}(CF) + \tau_0 \tag{11}$$

Here, η is the viscosity of the solvent in poise, V is the hydrodynamic volume of the probe molecule in m^3, k_B is the Boltzmann constant in J K^{-1}, and T is the absolute temperature, to give τ_{OR} in units of seconds. The free-rotor relaxation time, τ_0, given by $(2\pi/9)(I/k_BT)^{1/2}$, is generally of the order a few picoseconds, much shorter than diffusional motion in solvents of moderate viscosity, and is frequently omitted. Calculated values of τ_{OR} are generally within a factor of two or three of experimentally determined values although better estimates can be achieved using variations in DSE theory, where the coefficients f and C take on values related to probe shape and diffusion boundary conditions, respectively.[8–15] The hydrodynamic volume of RST can be estimated using several different methods. Considering RST as a general ellipsoid, its molecular dimensions[27] based on van der Waals diameters are $L = 16.1$Å, $M = 9.3$ Å, and $S = 3.9$ Å, and a volume of $V = 3.1 \times 10^{-28}$ m^3 is obtained. Utilizing the average density of aromatic hydrocarbons ($\rho \approx 0.88$ g/mL) and the molecular weight of RST leads to a volume of $V = 5.7 \times 10^{-28}$ m^3,

nearly a factor of two larger than the van der Waals diameters would suggest. It seems reasonable to assume that the hydrodynamic volume would be between these two limiting values. Numerical evaluation of τ_{OR} leads to values of $\tau_{OR} = 250$ to 500 ps in *n*-hexadecane at room temperature depending on which limiting value of the hydrodynamic volume is used. Clearly, DSE theory overestimates the reorientation lifetime under these conditions (Table 1). The theoretical values can be adjusted through convenient choices of the shape factor and boundary conditions, and several methods of estimating these correction factors have been proposed.[7]

It seems reasonable that the longer of the two experimentally observed time constants is due to random rotational motion, but it is still not clear if the shorter of the two time constants is consistent with such motion. Unfortunately, the uncertainty in the value of the hydrodynamic volume will persist regardless of which methods of evaluating f and C are used, and the determination of an absolute value for the time constant will be hampered by this fact. On the bright side, absolute values of the time constants are not required, but simply the ratio of the two time constants is all that is needed. Taking into account the shape factors of RST and the possible boundary conditions will be sufficient to determine the ratio of time constants, and determination of the hydrodynamic volume of the probe will not be required.

Ratio of Time Constants Based on Probe Shape and Boundary Conditions

It has been shown that the diffusion coefficients for rotation about each molecular axis can be linked by a function of the axial ratios of the probe.[28] The ratio of the diffusion coefficients for the principal axes of a general ellipsoid assuming stick boundary conditions can be scaled relative to the diffusion coefficient of a sphere of the same volume. In this context, the probe shape determines the scaling factors that will subsequently define the principal diffusion coefficients. If the probe shape is known, all of the exponential functions can be linked to a single adjustable parameter, D_0. According to the results of Small and Isenberg,[28] (see footnote 1), the rotational diffusion coefficients for the three molecular axes of RST will be given by $D_L = 0.93D_0$, $D_M = 0.44D_0$, and $D_S = 0.45D_0$ under stick boundary conditions. Using these diffusion coefficients, it is possible to calculate the expected ratio of time constants given by

$$\frac{\tau_2}{\tau_1} = \frac{6D + 2\Delta}{6D - 2\Delta} \tag{12}$$

[1]The tabulated diffusion coefficients from ref. 28 were plotted and the data interpolated to estimate the values at the axial ratios of RST.

where D and Δ are described in Eqs. (7) and (8). Notice that this ratio of time constants will be independent of the value of D_0 and therefore no longer dependent on the hydrodynamic volume assumed. Using the diffusion coefficients listed above, the ratio of the time constants for RST excited state under stick boundary conditions is predicted to be only $\tau_2/\tau_1 = 1.7$! The experimentally observed ratio of between 12 and 20 is well outside any reasonable prediction of the diffusion coefficients under stick conditions. We conclude that the observed time constants are not consistent with these boundary conditions.

A similar calculation is possible if slip boundary conditions are assumed. The rotational friction coefficients of the general ellipsoid under slip conditions have been tabulated by Youngren and Acrivos[29] and subsequently recalculated in their dimensionless form.[30] The tabulated values of the friction coefficients, λ_i, are related to the inverse of the rotational diffusion coefficients, which can be used to calculate D and Δ as was seen above. Given the rotational friction coefficients $\lambda_L = 2.63$, $\lambda_M = 9.12$, and $\lambda_S = 2.00$ at the slip boundary,[30] the ratio of the two time constants is expected to be only $\tau_2/\tau_1 = 2.1$. Again, it is apparent that the experimentally observed ratio of time constants cannot be consistent with the predictions of hydrodynamic theory for random rotational motion under slip boundary conditions either.

Are there any boundary conditions that can be defined which would allow the experimentally observed ratio of time constants to be rationalized? This question can be addressed if we return to the data sets for a more detailed analysis of the preexponential factors. Examination of the fit parameters collected in Table 1 reveals that when 355-nm excitation is used, the initial magnitude of the orientation factor is significantly different than the theoretical limits of 0.6 or 0.2 expected for a high-symmetry probe. This result suggests that there are overlapping transitions of different polarization in the ground state absorption spectrum of RST at 355 nm. The published analysis of the polarized ground state absorption spectrum of RST is consistent with this finding.[25] In contrast, when 404-nm excitation is used, the initial orientation factor approaches the theoretical limit of 0.6. This result suggests that the absorption at 404 nm in the ground state, as well as both of the transitions probed in the excited state, must be purely polarized and are parallel to each other. Once the theoretical limit has been observed for a set of excitation and probe wavelengths, additional information can be obtained by considering the magnitudes of the preexponential factors as given by Eqs. (13) and (14),

$$A_1 = \frac{\beta + \alpha}{15} \tag{13}$$

$$A_2 = \frac{\beta - \alpha}{15} \tag{14}$$

where

$$\beta = q_L^2\gamma_L^2 + q_M^2\gamma_M^2 + q_S^2\gamma_S^2 - \frac{1}{3} \tag{15}$$

$$\begin{aligned}\alpha = {} & \frac{D_L}{\Delta}\left(q_M^2\gamma_M^2 + q_S^2\gamma_S^2 - 2q_L^2\gamma_L^2 + q_L^2 + \gamma_L^2\right) \\ & + \frac{D_M}{\Delta}\left(q_L^2\gamma_L^2 + q_S^2\gamma_S^2 - 2q_M^2\gamma_M^2 + q_M^2 + \gamma_M^2\right) \\ & + \frac{D_S}{\Delta}\left(q_L^2\gamma_L^2 + q_M^2\gamma_M^2 - 2q_S^2\gamma_S^2 + q_S^2 + \gamma_S^2\right) - \frac{2D}{\Delta}\end{aligned} \tag{16}$$

The symbols q_i and γ_i represent the projections of the excitation and probe TMVs, respectively, onto the indicated molecular axis. The TMV projections are given by $q_{\mathrm{L}} = \cos\theta$, $q_{\mathrm{M}} = \sin\theta$, $\gamma_{\mathrm{L}} = \cos\phi$, and $\gamma_{\mathrm{M}} = \sin\phi$, where θ and ϕ represent the angle between the long hydrodynamic axis and the excitation and probe TMVs, respectively. For high-symmetry probes, such as RST, θ and ϕ must be either 0 or 90°. The polarized ground state spectrum shows that the TMV at 404 nm is directed along the long in-plane axis of RST.[26] The ground state TMV projections must therefore be $q_{\mathrm{L}} = 1$ and $q_{\mathrm{M}} = 0$, and the excited state TMV projections are required to be $\gamma_{\mathrm{L}} = 1$ and $\gamma_{\mathrm{M}} = 0$. With these TMV projections, β can be calculated, $\beta = 2/3$, and Eq. (16) reduces to:

$$\alpha = \frac{D - D_L}{\Delta} \tag{17}$$

The relationship between α and Δ given by Eq. (17) indicates that the ratio of time constants, which is dependent on Δ as shown Eq. (12), must also be related to the ratio of preexpontial factors, as defined using α and shown in Eq. (18).

$$\frac{A_1}{A_2} = \frac{2/3 + \alpha}{2/3 - \alpha} \tag{18}$$

In the specific case of the RST dichroism decays recorded using 404-nm excitation, the observed ratio of time constants is large, requiring Δ to be large. At the same time, the observed weights of the two exponentials are nearly equal, which requires α to be small. Is it physically possible for random rotational diffusion to allow large differences in time constants yet have similar weights of the two exponentials within the decay? In other words, according to models of random diffusional motion, is it possible for Δ to be large and α to be small at the same time?

According to Eq. (18) it is clear that the ratio of preexponential factors will approach 1 only when α approaches zero. Equation (17) shows that α approaches zero only when $D - D_{\mathrm{L}}$ approaches zero. There are two limiting cases where $D - D_{\mathrm{L}} = 0$. The first of these is the isotropic limit where $D_{\mathrm{L}} = D_{\mathrm{M}} = D_{\mathrm{S}} = D$, in which case Δ also approaches zero and both time

constants are equal (see footnote 2). The second limit requires values of D_M (or D_s) = 0, and D_S (or D_M) = $2D$. In this case, α again approaches zero, but Δ approaches a maximum value of only $\sqrt{3}$D. Therefore, the largest ratio of time constants that can be expected when the ratio of preexponential factors is 1 is $\tau_2/\tau_1 = 3.7$. We are left to conclude that for purely polarized transitions, there are no physically allowed combinations of diffusion coefficients, consistent with any boundary conditions or probe shapes, where random rotational diffusion can lead to a ratio of time constants greater than 3.7 with equal weights of the preexponential factors.

The observed time-constants for RST in *n*-hexadecane cannot both be due to random diffusional motion. DSE theory suggests that the longer time constant, ca. $\tau_2 \approx 180$ ps, may be due to random rotational motion and is therefore likely to be a weighted average of two exponential decay terms as hydrodynamic theory requires. We can only speculate about the identity of the fast component. It is likely that solvent polarization, vibrationally hot rotations, rapid structural changes on the excited surface, or some combination of these processes is responsible for the appearance of the $\tau_1 \approx 12$ ps decay. Similar phenomena have been postulated in the case of a very rapid initial decay for perylene[17,18] and for coumarin 153,[20] among others.[17]

It becomes clear why reorientational diffusion is frequently described accurately using only single exponential model functions.[16,19,20] When the time constants are significantly different, one of them will dominate the observed dichroism decay. Conversely, when both time constants can be expected to have similar weights within the decays, the time constants must be nearly equal.

The RST data presented here is unique in that the limiting value of the orientation factor was observed, and therefore the starting orientation of the excited probes, on average, is well understood. When the theoretically limiting values of the orientation factors are not observed, the analysis of the preexponential factors requires a detailed understanding of the process(es) that are responsible for the loss of apparent orientation, which is not readily available in general. However, when the limiting orientation factors are not observed, it is possible to obtain two significantly different time constants with similar weights within the decays if there are overlapping transitions of differing polarization at the excitation or probe wavelengths. Examples of this type of exception may include perylene in several solvents.[15,17,18]

We conclude that the rotational dynamics of RST include (at least) two exponential terms in the description of the orientation decay but that it is unlikely that both of the observed decay processes can be described by random diffusional motion regardless of the boundary conditions assumed.

[2]It is important to consider the magnitudes of the quantities $D - D_L$ and Δ as the isotropic limit is approached. Near the isotropic limit, $D - D_L$ must approach zero faster than does Δ if Eq. (17) is valid. Thus, for isotropic diffusion, the ratio of time constants approaches unity and both Δ and α must approach zero.

ACKNOWLEDGMENTS

Support for this work by the University of Maryland, Baltimore County, and NSF (CHE-9985299) is gratefully acknowledged. D.L. also acknowledges NIH for support through a Chemistry-Biology Interface Training Grant (T37 GM066706).

REFERENCES

1. Lakowicz, J. R. *Principles of Fluorescence Spectroscopy*, 2nd Ed.; Kluwer Academic/Plenum: New York, 1999, pp. 291–366.
2. Thulstrup, E. W.; Michl, J. *Spectroscopy with Polarized Light. Solute Alignment by Photoselection in Liquid Crystals, Polymers and Membranes*; VCH Publishers: Deerfield Beach, 1986.
3. Thulstrup, E. W.; Michl, J. *Elementary Polarization Spectroscopy*; VCH Publishers: Deerfield Beach, 1989.
4. Ansari, A.; Szabo, A. Theory of photoselection by intense laser pulses. Influence of reorientational dynamics and chemical kinetics on absorbance measurements. *Biophys. J.* **1993**, *64*, 838–851.
5. Szabo, A. Theory of fluorescence depolarization in macromolecules and membranes. *J. Chem. Phys.* **1984**, *81*, 150–167.
6. Magde, D. Photoselection with intense laser pulses. *J. Chem. Phys.* **1978**, *68*, 3717–3733.
7. Fleming, G. R. *Chemical Applications of Ultrafast Spectroscopy*; Oxford University Press: New York, 1986, Chapter 6, pp. 155–200.
8. (a) Sension, R. J.; Repinec, S. T.; Hochstrasser, R. M. Femtosecond laser study of the alignment of reactant and products in the photoisomerization reactions of cis-stilbene. *J. Phys. Chem.* **1991**, *95*, 2946–2948; (b) Repinec, S. T.; Sension, R. J.; Szarka, A. Z.; Hochstrasser, R. M. Femtosecond laser studies of the cis-stilbene photoisomerization reactions. The cis-stilbene to dihydrophenanthrene reaction. *J. Phys. Chem.* **1991**, *95*, 10380–10385; (c) Sension, R. J.; Repinec, S. T.; Szarka, A. Z.; Hochstrasser, R. M. Femtosecond laser studies of the cis-stilbene photoisomerization reactions. *J. Phys. Chem.* **1993**, *98*, 6291–6315.
9. Arnold, B. R.; Schill, A. W.; Poliakov, P. P. Application of time-resolved linear dichroism spectroscopy: relaxation of excited hexamethylbenzene/1,2,4,5-tetracyanobenzene charge-transfer complexes. *J. Phys. Chem. A* **2001**, *105*, 537–543.
10. Barkley, M. D.; Kowalczyk, A. A.; Brand, L. Fluorescence decay studies of anisotropic rotations of small molecules. *J. Chem. Phys.* **1981**, *75*, 3581.
11. Singh, M. K. Rotational relaxation of neutral red in alkanes: effect of solvent size on probe rotation. *Photochem. Photobiol.* **2000**, *72*, 438–443.
12. Bessire, D. R.; Quitevis, E. L. Effect of temperature and viscosity on rotational diffusion of Merocyanine 540 in polar solvents. *J. Phys. Chem.* **1994**, *98*, 13083–13092.
13. Ho, N.; Kajimoto, O.; Hara, K. High-pressure studies of rotational dynamics for Coumarin 153 in alcohols and alkanes. *J. Phys. Chem. A* **2002**, *106*, 6024–6029.
14. (a) Brocklehurst, B.; Young, R. N. Rotation of aromatic hydrocarbons in viscous alkanes. 1. methylcyclohexane. *J. Phys. Chem. A* **1999**, *103*, 3809–3817; (b) Brocklehurst, B.; Young, R. N. Rotation of aromatic hydrocarbons in

viscous alkanes. 2. hindered rotation in squalane. *J. Phys. Chem. A* **1999**, *103*, 3818–3824.
15. Jas, G. S.; Larson, E. J.; Johnson, C. K.; Kuczera, K. Microscopic details of rotational diffusion of perylene in organic solvents: molecular dynamics simulation and experiment vs Debye-Stokes-Einstein theory. *J. Phys. Chem. A* **2000**, *104*, 9841–9852.
16. Benzler, J.; Luther, K. Rotational relaxation of biphenyl and p-terphenyl in n-alkanes: the breakdown of the hydrodynamic description. *Chem. Phys. Lett.* **1997**, *297*, 333–338.
17. Szubiakowski, J.; Balter, A.; Nowak, W.; Kowalczyk, A.; Wisniewski, K.; Wierzbowska, M. Anisotropic reorientation of perylene and 3,9-dibromoperylene in glycerol: fluorescence anisotropy decay and quantum-mechanical study. *Chem. Phys.* **1996**, *208*, 283–296.
18. Xu, J.; Shen, X.; Knutson, J. R. Femtosecond fluorescence upconversion study of the rotations of perylene and tetracene in hexadecane. *J. Phys. Chem. A* **2003**, *107*, 8383–8387.
19. Hartman, R. S.; Alavi, D. S.; Waldeck, D. H. An experimental test of dielectric friction models using the rotational diffusion of aminoanthraquinones. *J. Chem. Phys.* **1991**, *95*, 7872–7880.
20. Horng, M.-L.; Gardecki, J. A.; Maroncelli, M. Rotational dynamics of coumarin 153: time-dependent friction, dielectric friction, and other nonhydrodynamic effects. *J. Phys. Chem. A* **1997**, *101*, 1030–1047.
21. Belford, G. G.; Belford, R. L.; Weber, G. Dynamics of fluorescence polarization in macromolecules. *Proc. Nat. Acad. Sci.* **1972**, *69*, 1392–1393.
22. Chuang, T. J.; Eisenthal, K. B. Theory of fluorescence depolarization by anisotropic rotational diffusion. *J. Chem. Phys.* **1972**, *57*, 5094–5097.
23. Arnold, B. R.; Schill, A. W. Rotational dynamics of excited probes: the analysis of experimental data. *Spec. Lett.* **2002**, *35*, 229–238.
24. Poliakov, P.; Arnold, B. R. An application of time-resolved linear dichroism spectroscopy: the excited singlet state of 1,2:5,6-dibenzanthracene. *Spec. Lett.* **1999**, *32*, 747–762.
25. Pedersen, P. B.; Thulstrup, E. W.; Michl, J. Magnetic circular dichroism of cyclic pi- electron systems. 24. polarizations and assignments in some pentacyclic and hexacyclic benzenoid hydrocarbons. *Chem. Phys.* **1981**, *60*, 187–198.
26. Hodgkinson, K. A.; Munro, I. H. Excited singlet state and triplet states of aromatic hydrocarbons determined by a laser flash photolysis technique. *J. Molec. Spec.* **1973**, *48*, 57–71.
27. Sander, L. C.; Wise, S. A. *Polycyclic Aromatic Hydrocarbon Structure Index*, NIST Special Publication 922; U.S. Government Printing Office: Washington, D.C., 1997.
28. Small, E. W.; Isenberg, I. Hydrodynamic properties of a rigid molecule: rotational and linear diffusion and fluorescence anisotropy. *Biopolymers* **1977**, *16*, 1907–1928.
29. Youngren, G. K.; Acrivos, A. Rotational friction coefficients for ellipsoids and chemical molecules with the slip boundary condition. *J. Chem. Phys.* **1975**, *63*, 3846–3848.
30. Sension, R. J.; Hochstrasser, R. M. Comment on: rotational friction coefficients for ellipsoids and chemical molecules with slip boundary conditions. *J. Chem. Phys.* **1993**, *98*, 2490.